

Electrostatic Attractive Self-Delivery of siRNA and Light-Induced Self-Escape for Synergistic Gene Therapy

Yuxin Yang, Haijun Ning, Tianping Xia, Jianjun Du, Wen Sun, Jiangli Fan,* and Xiaojun Peng

Small interfering RNA (siRNA) holds immense promise for suppressing gene expression and treating various life-threatening diseases, including cancer. However, efficient delivery and lysosomal escape remain critical challenges that hinder the therapeutic effectiveness of siRNA. Herein, cationic photosensitizer (NB-Br) is grafted onto polo-like kinase 1 (PLK1) siRNA to form an amphiphilic siRNA-photosensitizer conjugate (siPLK1-NB), which can self-assemble into nanoparticles (siPLK1-NB NPs) via electrostatic attraction. Notably, siPLK1-NB NPs exhibit rapid and efficient cell endocytosis, as well as outstanding tumor-targeting property in multiple tumor-bearing mice models. When siPLK1-NB NPs are located inside tumor cell lysosomes, the generated reactive oxygen species (ROS) after photoactivation can disrupt the lysosome membrane structure and facilitate siRNA escape from lysosomes. Under light irradiation, siPLK1-NB NPs can downregulate PLK1 expression and induce photodynamic killing, effectively inhibiting tumor cell growth both *in vitro* and *in vivo*. Consequently, this study provides a novel design strategy for carrier-free siRNA delivery systems. As far as it is known, this is the first report of a carrier-free siRNA delivery system based on electrostatic attraction.

1. Introduction

RNA interference (RNAi), including microRNA and small interfering RNA (siRNA), has emerged as a promising gene regulatory strategy that can specifically target and silence disease-related genes, holding great promise for treating a variety of life-threatening diseases and providing better options for traditional small molecule therapies.^[1,2] Thereof, siRNA, a class

of exogenous double-stranded RNA molecules, has performed superior efficiency and specificity in the clinical treatments, such as acute hepatic porphyria, primary hyperoxaluria type I, hypercholesterolemia, and cancer.^[3] Theoretically, siRNA has the ability to downregulate any gene and further controlling protein expression in a sequence-dependent manner.^[4] However, on the one hand, owing to its hydrophilic and polyanionic property, naked siRNA is unable to cross the cell membrane and is easily degraded by ribonucleases, resulting in minimal therapeutic activity.^[5–7] To address these challenges, various delivery carriers have been explored in depth, including viral vectors,^[8] cationic polymers,^[9] liposomes,^[10] and porous organic/inorganic nanoparticles (NPs),^[11] promoting siRNA to cross biological barriers and prolonging the blood circulation. Although Patisiran (ONPAT-TROTM), a lipid-based siRNA drug, has been commercialized for the treatment of

polyneuropathies since 2018,^[12] these carriers still face tedious preparation, drug loading capacity, stability, and biosafety issues. On the other hand, carrier-mediated delivery systems are generally facilitating cellular entry via endocytosis and entrapped in endosomes.^[13–15] The endosomes then fuse with the lysosomes, leading to reduced or even no release of oligonucleotide drugs (ONDs) in the cytosol to induce gene silence.^[16,17] Cationic polymers, such as polyethyleneimine (PEI), have been used to facilitate endo/lysosome escape through the proton sponge effect.^[18] However, owing to their high positive charge density, cationic nanoparticles may induce the intense interactions with negatively charged serum proteins and cellular membrane disruption,^[19] leading to the instability and rapid clearance of nanocarriers during circulation, thereby reducing the clinical efficacy of siRNA.^[20] In recent years, carrier-free drug delivery systems have risen for ONDs delivery, which could avoid the biosafety risks due to using extra polymeric components. Zhang et al.^[21] reported a carrier-free drug-chemogene conjugate for synergistic tumor treatment, which grafted two hydrophobic paclitaxel with a hydrophilic flouxuridine-integrated antisense oligonucleotide to construct an amphiphilic conjugate, laying the foundation for carrier-free ONDs delivery systems. However, multiple components and complex preparation steps were used to conduct this delivery system. Moreover, carrier-free delivery

Y. Yang, H. Ning, T. Xia, J. Du, W. Sun, J. Fan, X. Peng
State Key Laboratory of Fine Chemicals
Frontiers Science Center for Smart Materials Oriented Chemical

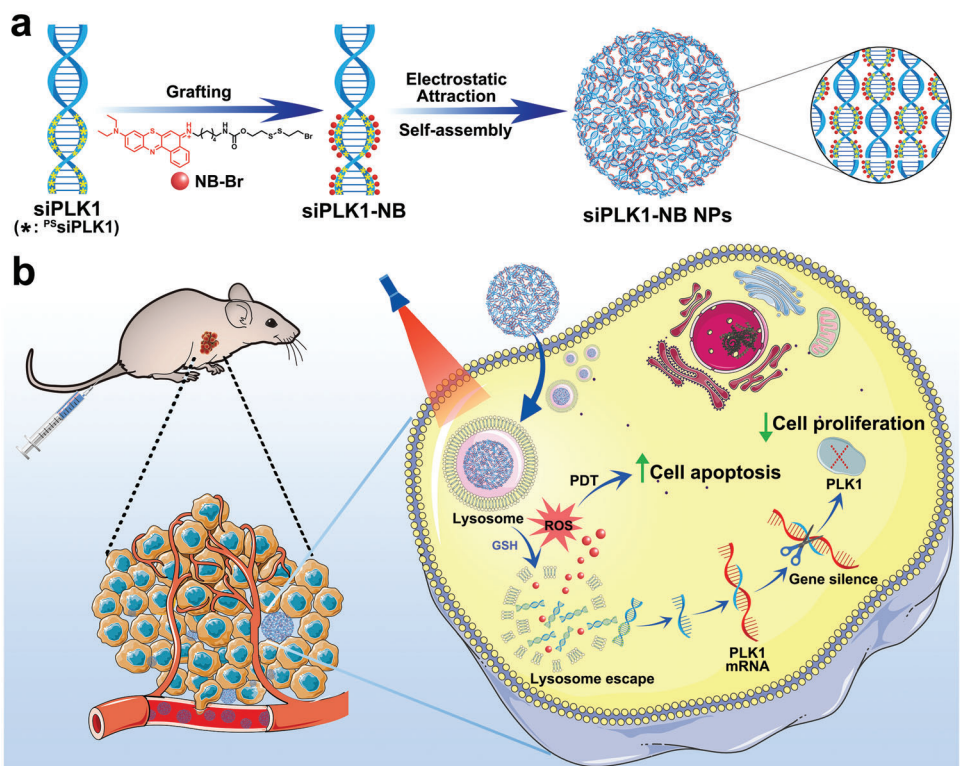
Engineering
Dalian University of Technology
Dalian 116024, China
E-mail: fanjl@dlut.edu.cn

J. Du, W. Sun, J. Fan
Ningbo Institute of Dalian University of Technology
Ningbo 315016, China

X. Peng
Research Institute of Dalian University of Technology in Shenzhen
Gaoxin South Fourth Road, Nanshan District, Shenzhen 518057, China

 The ORCID identification number(s) for the author(s) of this article can be found under <https://doi.org/10.1002/adma.202301409>

DOI: 10.1002/adma.202301409



Scheme 1. a) Schematic representation of the preparation of siPLK1-NB conjugate, and the self-assembly of siPLK1-NB NPs. b) Schematic illustration of the cellular uptake and intracellular trafficking of siPLK1-NB NPs for synergistic gene therapy.

systems for siRNA are still lacking. Therefore, further exploration of novel and facile strategies to construct carrier-free delivery systems capable of lysosome escape is of great significance for siRNA nanomedicine.

As a noninvasive treatment modality, photodynamic therapy (PDT) has emerged as a promising treatment for cancer.^[22–24] When photosensitizers (PSs) are internalized by cells and entrapped in lysosomes, the reactive oxygen species (ROS) generated by PSs upon photoactivation can destroy the endo/lysosome membrane and thus facilitate siRNA escape from lysosomes.^[25] In recent decades, the chemical modification of the phosphodiester linkage by replacing a nonbridging oxygen with a sulfur atom has been extensively utilized for improving the stability of ONDs.^[26] And the nucleophilicity of the sulfur atom in the phosphorothioate group (PS) is much stronger than the oxygen atom in the phosphodiester group (PO), enabling it to react with electrophilic reagents like alkyl halides.^[18,27] Previously, our group has developed a cationic photosensitizer, sulfur-substituted Nile Blue, which is capable of generating a considerable amount of $O_2^{•-}$ under the irradiation of near-infrared (NIR) light for tumor PDT.^[28,29] Taking these considerations into account, we developed a brominated sulfur-substituted Nile Blue (abbreviated as NB-Br) with glutathione-responsive property to conjugate with phosphorothioate group, which could be accumulated preferentially in the lysosome.

Then, for the first time, we designed a carrier-free delivery system (siPLK1-NB NPs) based on electrostatic attraction to achieve self-delivery and NIR-induced lysosome escape for siRNA drugs.

Polo-like kinase 1 (PLK1), which is typically overexpressed in most cancer cells and plays a critical role in regulating the process of mitosis in mammalian cells, was chosen as the targeted gene for RNAi therapy.^[20,30,31] In brief, by utilizing a deblock design of siPLK1 strands that consists of both ^{PO}siPLK1 segments and ^{P5}siPLK1 segments (Table S1, Supporting Information), the NB-Br was specifically grafted onto the ^{P5}siPLK1 segments through nucleophilic addition elimination reaction. After the multitude of grafting reactions, the ^{P5}siPLK1 segments became highly positively charged, while the ^{PO}siPLK1 segments remained negatively charged, resulting in the formation of amphiphilic siPLK1-NB conjugations that could self-assemble into nanoparticles and achieve carrier-free delivery (Scheme 1). Consequently, without the aid of any extra components, siPLK1-NB NPs demonstrated good physiological stability and rapid cell endocytosis with simple preparation. Upon uptake by tumor cells, because of the cleavage of disulfide linker by overexpressed glutathione (GSH) in the tumor microenvironment,^[32,33] siPLK1-NB NPs would disintegrate and then release siPLK1 and photosensitizers. Profiting from photochemical internalization, the generated ROS significantly promoted siPLK1 escape from lysosomes and further achieve the RNAi and PDT synergistic cancer treatment. Owing to the enhanced permeability and retention (EPR) effect and the unbalanced internal charge, siPLK1-NB NPs exhibited outstanding tumor-targeting property *in vivo*.^[34] As a result, siPLK1-NB NPs demonstrated effective siRNA delivery and anticancer efficacy, providing a novel design principle for carrier-free siRNA delivery systems.

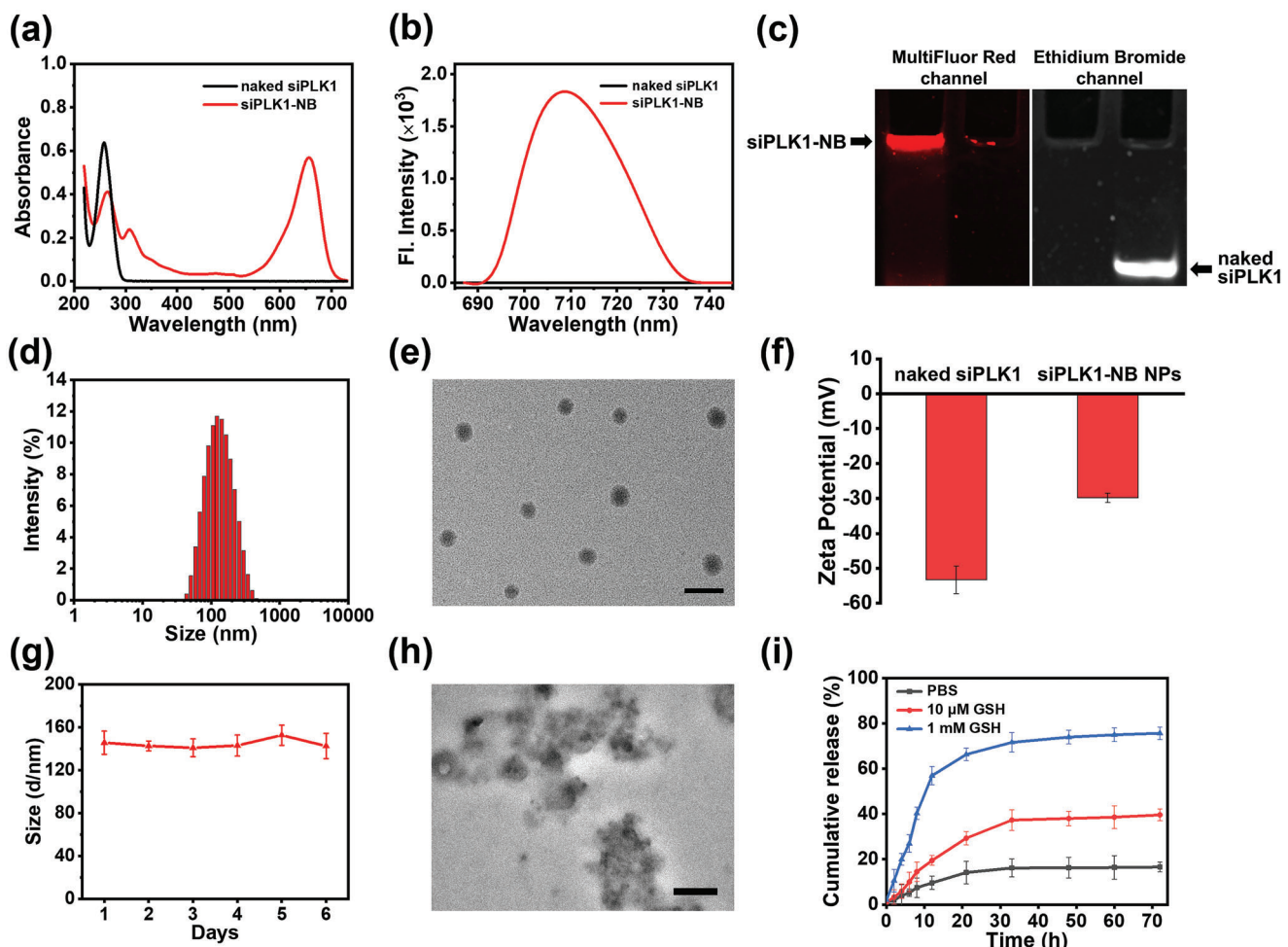


Figure 1. Characterization of NB-grafted siPLK1 and siPLK1-NB NPs. a) Absorption spectra and b) fluorescence spectra of naked siPLK1 and siPLK1-NB conjugates. c) 20% of non-denaturing PAGE gel image of naked siPLK1 and siPLK1-NB conjugates. siPLK1-NB could quench the fluorescent signals of EB under FluorChem E imaging system. Hence, siPLK1-NB was imaged under MultiFluor Red channel. d) The diameter of the siPLK1-NB NPs measured using DLS. e) TEM image of siPLK1-NB NPs. Scale bar: 300 nm. f) Zeta potential of naked siPLK1 and siPLK1-NB NPs. g) The stability study of siPLK1-NB NPs in PBS buffer. h) TEM image of siPLK1-NB NPs after incubated with 1 mM GSH for 1 h. Scale bar: 200 nm. i) In vitro drug release at 37 °C in PBS, PBS with 10 μ M GSH, and PBS with 1 mM GSH, respectively. Error bars: mean \pm standard deviation (SD) ($n = 3$).

2. Results and Discussion

First, NB-Br was synthesized and the experimental details are shown in Scheme S1 (Supporting Information). The chemical structure of NB-Br was fully characterized by ^1H NMR, ^{13}C NMR, and HR-MS analytical data (Figures S1–S3, Supporting Information). NB-Br displayed a maximum absorption peak at 660 nm, laying in the therapeutic window, and exhibited high NIR fluorescence at 700 nm. To confirm the photosensitizing efficiency of NB-Br, the ROS probe dihydrorhodamine 123 (DHR123) was used, which emits strong green fluorescence after reacting with $\text{O}_2^{-\bullet}$.^[35] Within 10 min of irradiation, NB-Br significantly increased the fluorescence intensity of DHR123, exhibiting excellent photosensitizing efficiency (Figure S4, Supporting Information).

To conduct the siPLK1-NB conjugate, NB-Br and siPLK1 were dissolved in DMSO and vibrated at 50 °C for 48 h. After the reaction, unreacted NB-Br was removed by the ethanol precipita-

tion method, followed by purification using a dialysis tube. Unlike naked siPLK1, siPLK1-NB displayed an extra absorption peak centered at 660 nm and NIR fluorescence centered at 708 nm (Figure 1a,b). The successful synthesis of siPLK1-NB was confirmed by the matrix-assisted laser desorption/ionization time-of-flight mass spectrometry (MALDI-TOF MS), which showed that the molecular weight of siPLK1 increased from 7809.2 to 20 351.2 and 15 004.4 to 28 575.0, respectively (Figures S5, Supporting Information). The amounts of NB-Br grafted onto siPLK1 were \approx 21 and 23, respectively, which is basically consistent with the theoretical value (22 and 23). Moreover, 20% non-denaturing polyacrylamide gel electrophoresis (PAGE) was applied to characterize the mobility of siPLK1-NB conjugate. Compared to the naked siPLK1, the siPLK1-NB was entrapped in the loading well since the large assemblies formed (Figure 1c), indicating the successful conjugation of NB-Br to siPLK1.

As a large amount of NB-Br grafting on the ps siPLK1 segments, the ps siPLK1 segments were highly positively charged,

while the ^{PO}siPLK1 segments remained negatively charged, contributing to the formation of amphiphilic siPLK1-NB conjugates. siPLK1-NB could self-assemble into siPLK1-NB NPs in aqueous solution under sonication. To further investigate the intermolecular interaction in siPLK1-NB, molecular docking simulation was performed. As shown in Figure S6 (Supporting Information), the two nitrogen atoms in NB-Br could form hydrogen bonds with the siPLK1 bases, and the lengths of hydrogen bonds were 1.7 and 2.5 Å, respectively. However, compared to the electrostatic attraction, the hydrogen bonding here was weaker interaction. Thus, the formation of siPLK1-NB NPs was primarily driven by electrostatic attraction. The hydrodynamic size of siPLK1-NB NPs determined by dynamic light scattering (DLS) was \approx 144 nm with a low polydispersity index (PDI) of 0.036 (Figure 1d). Transmission electron microscopy (TEM) images showed the spherical morphology of siPLK1-NB NPs with an average diameter of \approx 120 nm, confirming their self-assembly into nanoparticles (Figure 1e). In addition, the zeta potential of naked siPLK1 was negatively charged, but the zeta potential of siPLK1-NB NPs underwent a charge increase from -53.3 to -29.8 mV (Figure 1f), indicating successful conjugation between NB-Br and siPLK1. It is worth noting that the size of siPLK1-NB NPs remained nearly unchanged after storage in phosphate buffered saline (PBS) for 6 days, demonstrating the good stability (Figure 1g). Then, siPLK1-NB NPs were incubated with Dulbecco's modified Eagle medium (DMEM) culture medium containing 10% fetal bovine serum (FBS) or 1 μ g mL⁻¹ RNase A at 37 °C and characterized by agarose gel electrophoresis (Figure S7, Supporting Information). After being incubated with DMEM (10% FBS) for 6 h, siPLK1-NB NPs could run into the agarose gel and appeared as a sharp band, indicating its good stability in a physiological environment. Moreover, in contrast to naked siPLK1, most of siPLK1-NB NPs remained intact even after being incubated with 1 μ g mL⁻¹ RNase A for 2 h, demonstrating that the novel architecture indeed could protect the siRNA from degradation by ribonucleases (Figure S7, Supporting Information), which is essential for delivery systems.

Intact PSs can be released by the GSH-responsive cleavage of the disulfide linker.^[32] Upon incubation with 1 mM GSH for 1 h, as shown in Figure 1h, siPLK1-NB NPs displayed a broken structure, suggesting the GSH-responsive disassembly. Meanwhile, the dialysis method was used to analyze the PSs release behavior from siPLK1-NB NPs. Only 18% of PSs were released following a 72 h incubation in PBS without GSH. In contrast, in the presence of 1 mM GSH, \approx 80% of PSs were released, demonstrating the GSH-responsive drug release profile of siPLK1-NB NPs.

The cellular uptake efficiency of siPLK1-NB NPs in HepG2 cells was determined by confocal laser scanning microscopy (CLSM) and flow cytometry. With prolonged incubation time, the red fluorescence of siPLK1-NB increased in a time-dependent manner (Figure 2a). Subsequently, the cellular uptake efficiency of siPLK1-NB NPs was evaluated using flow cytometry analysis. As shown in Figure 2a,b, the siPLK1-NB NPs exhibited a time- and concentration-dependent cellular uptake behaviors. Even when incubated at a low concentration of 0.2 μ M, or for a short time of only 0.5 h, siPLK1-NB NPs exhibited remarkably fluorescent signals, suggesting the rapid internalization of siPLK1-NB NPs. However, even after 6 h of incubation, naked siRNA could still hardly be internalized by HepG2 cells compared to siPLK1-NB NPs (Figure 2c). It has been reported that the mod-

ification of ONs with disulfide units could enhance the cellular uptake of ONs.^[36] By introducing the disulfide linker and Nile blue, which has an affinity for lipophilic molecules,^[37] siPLK1-NB NPs displayed effective cellular uptake, suggesting the ability as an efficient carrier-free gene delivery system.

After that, 2',7'-dichlorofluorescin diacetates (DCFH-DA), a typical fluorescent ROS probe indicator in living cells, was used to monitor the ROS by CLSM. In contrast to the group without 660 nm irradiation, cells treated with siPLK1-NB NPs and irradiation displayed intense fluorescence (Figure S8, Supporting Information), indicating the sufficient intracellular ROS generation efficacy of siPLK1-NB NPs. Then, the intracellular distribution of siPLK1-NB NPs was studied using a commercial lysotracker. As shown in Figure 2d, under dark conditions, the red fluorescence of siPLK1-NB NPs overlapped well with the signal of LysoTracker Green DND 26 (green fluorescence) with a high Pearson's correlation coefficient of 0.812 in 6 h, demonstrating that a great majority of siPLK1-NB NPs were trapped in the lysosomes. Except for cellular internalization, lysosome escape is regarded as one of the most serious obstacles for RNAi therapy. Previous studies have demonstrated that ROS can destroy the membrane components, thus allowing siRNA to escape from the endosomes/lysosomes.^[4,38] In our case, it could be observed that after incubation of HepG2 cells with siPLK1-NB NPs for 6 h and then treated under 660 nm light irradiation (15 mW cm⁻², 5 min), the red fluorescence signal of siPLK1-NB NPs escaped from lysosomes, as evidenced by the Pearson's coefficient, which decreased to 0.470.

Then, the in vitro cell viability of HepG2, MCF-7 and 4T1 cells was evaluated after incubation with siPLK1-NB NPs by the methyl thiazolytetrazolium (MTT) assay (Figure 3a). Here, scrambled siRNA was utilized as a negative control to distinguish sequence-specific silence from non-specific effects, which was prepared into scrRNA-NB NPs through the same preparation method as siPLK1-NB NPs. No obvious cytotoxicity was observed when 250 nM of scrRNA-NB NPs were incubated without light irradiation, and the HepG2 cells' survival rate was close to 84%, suggesting the good biocompatibility. Upon exposure to 660 nm light (15 mW cm⁻², 10 min), scrRNA-NB NPs exhibited significant phototoxicity and the cell viability was dropped to 36%. Meanwhile, under dark conditions, when 250 nM of siPLK1-NB NPs were used, the growth of HepG2 cells was inhibited by \approx 40%, which was attributed to siPLK1-mediated gene therapy. Under light irradiation (660 nm, 15 mW cm⁻², 10 min), the cell viability of siPLK1-NB NPs treated group was only 18%. These results well demonstrated that siPLK1-NB NPs exhibited excellent advantages of synergistic gene-PDT therapy. Similar results were observed in MCF-7 and 4T1 cells as well. Additionally, the cell apoptosis assay was evaluated using an Annexin V-FITC/PI detection kit (Figure 3b; Figure S9, Supporting Information). HepG2 cells treated with siPLK1-NB NPs (200 nM) under 660 nm irradiation (15 mW cm⁻²) for 5 min showed significantly higher rates of cell apoptosis/necrosis (18.85% or 34.81%) than other groups. These results confirmed the advantages of synergy gene-PDT therapy by conducting siPLK1-NB NPs as a carrier-free delivery system.

siRNA regulates the expression of specific genes by degrading mRNA after transcription, which in-turn inhibits translation of the protein.^[39] Subsequently, the mRNA expression levels of

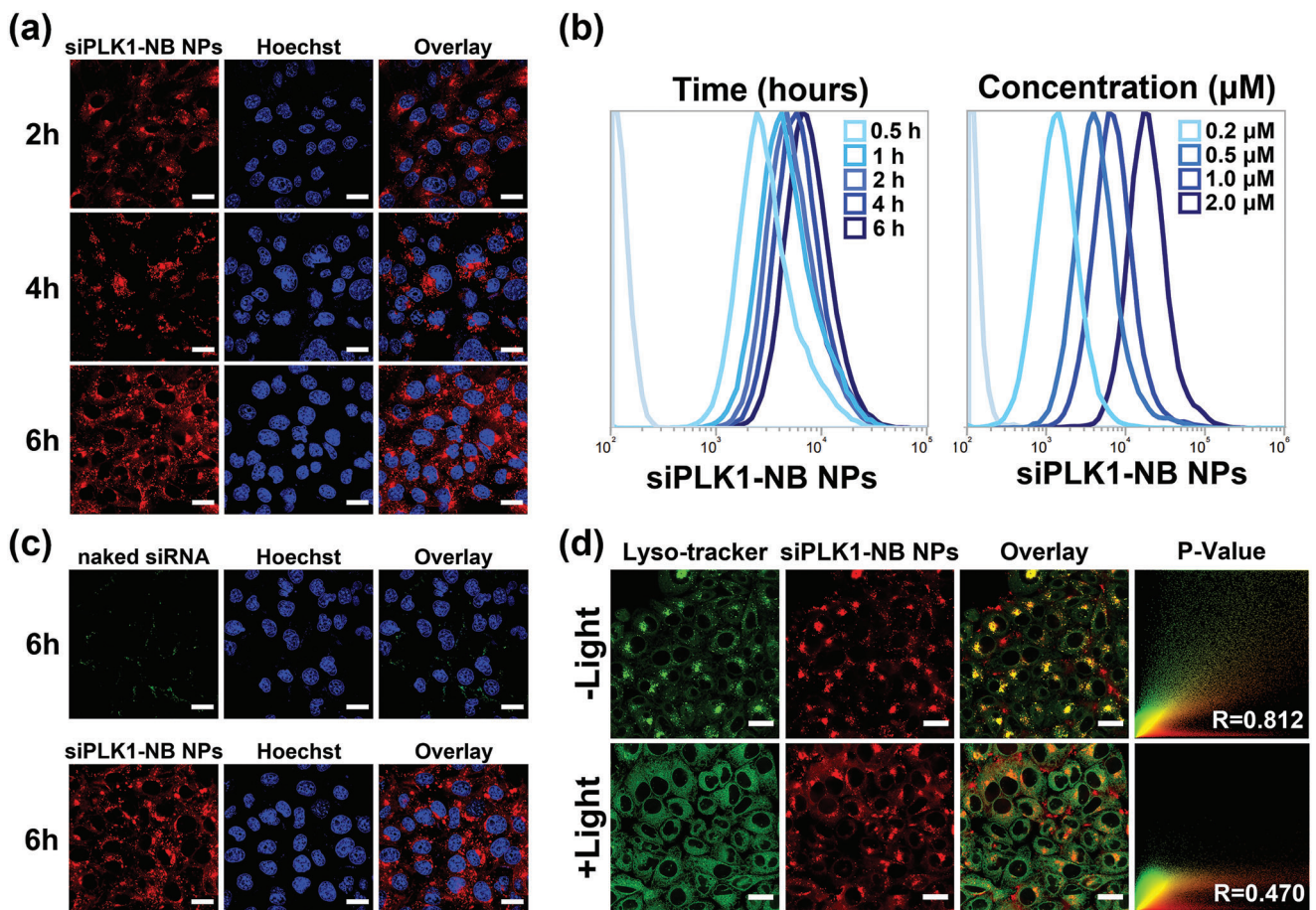


Figure 2. Cellular uptake and lysosome escape of siPLK1-NB NPs. a) CLSM images of HepG2 cells after incubated with the siPLK1-NB NPs for different durations. Scale bars: 20 μ m. b) Flow cytometry analysis of HepG2 cells incubated with siPLK1-NB NPs for different durations at 1 μ M and at different concentrations for 6 h, respectively. c) Confocal fluorescence images of HepG2 cells after incubation with naked siRNA and siPLK1-NB NPs for 6 h. Scale bars: 20 μ m. d) Confocal imaging study of HepG2 cells co-staining with Lysotracker Green and siPLK1-NB NPs. R is the correlation coefficient. Scale bars: 20 μ m.

the PLK1 gene were evaluated using quantitative real-time polymerase chain reaction (qRT-PCR) (Figure 3c). As expected, neither naked siPLK1 nor scrRNA-NB NPs cause any regulation of PLK1 mRNA levels. At a siPLK1 concentration of 150 nm and a 660 nm (15 mW cm^{-2}) irradiation time of 5 min, the PLK1 mRNA expression level in HepG2 cells being incubated with siPLK1-NB NPs was decreased by 35%, surpassing the efficacy of lipofectamine 2000 (a commercial transfection agent). Western blot analysis further confirmed that the siPLK1-NB NPs treated group under irradiation had remarkably downregulated PLK1 protein level (Figure 3d). These results also indicated that the moderate ROS production from siPLK1-NB NPs could facilitate lysosome escape without affecting the intracellular function of siPLK1.

Based on the encouraging in vitro results, we further studied the tumor-targeting potential and biodistribution of siPLK1-NB NPs. It is reported that NPs with 10 to 200 nm diameters can accumulate at tumor sites benefitting from the EPR effect and the tissue-specific delivery can be mediated by internal and/or external charge adjustment.^[34] In our case, siPLK1-NB NPs displayed an unbalanced internal charge and an average hydrodynamic diameter of 144 nm owing to the cationic NB-Br grafting on siPLK1.

Therefore, 4T1-tumor-bearing BALB/c mice were intravenously injected with siPLK1-NB NPs, FAM-labeled naked siPLK1 and NB-Br, respectively, which were then determined by an in vivo animal imaging system at different time points. As shown in Figure 4a, in contrast to the free NB-Br and naked siPLK1 groups, the significant fluorescent signal of siPLK1-NB NPs at the tumor site rapidly increased and peaked at 1 h post-injection, exhibiting excellent tumor-targeting potential. Subsequently, tumors and major organs were collected at 1 h post-injection for quantitative analysis of the biodistribution of siPLK1-NB NPs. As shown in Figure 4b, the siPLK1-NB NPs treated group displayed much stronger fluorescence in the tumor tissue compared to the free NB-Br and naked siPLK1 groups. Notably, tumor accumulation in the siPLK1-NB NPs group was 5.23 times higher than that in the naked siPLK1 group (Figure 4c), indicating the excellent tumor-targeting ability of siPLK1-NB NPs. Cell derived xenograft (CDX) tumor models are more accurately reflective of human tumor growth conditions. Hence, tumor-xenografted athymic nude mouse models were further subjected to in vivo optical imaging and an ex vivo biodistribution study, including MDA-MB-231-tumor-bearing, MCF-7-tumor-bearing

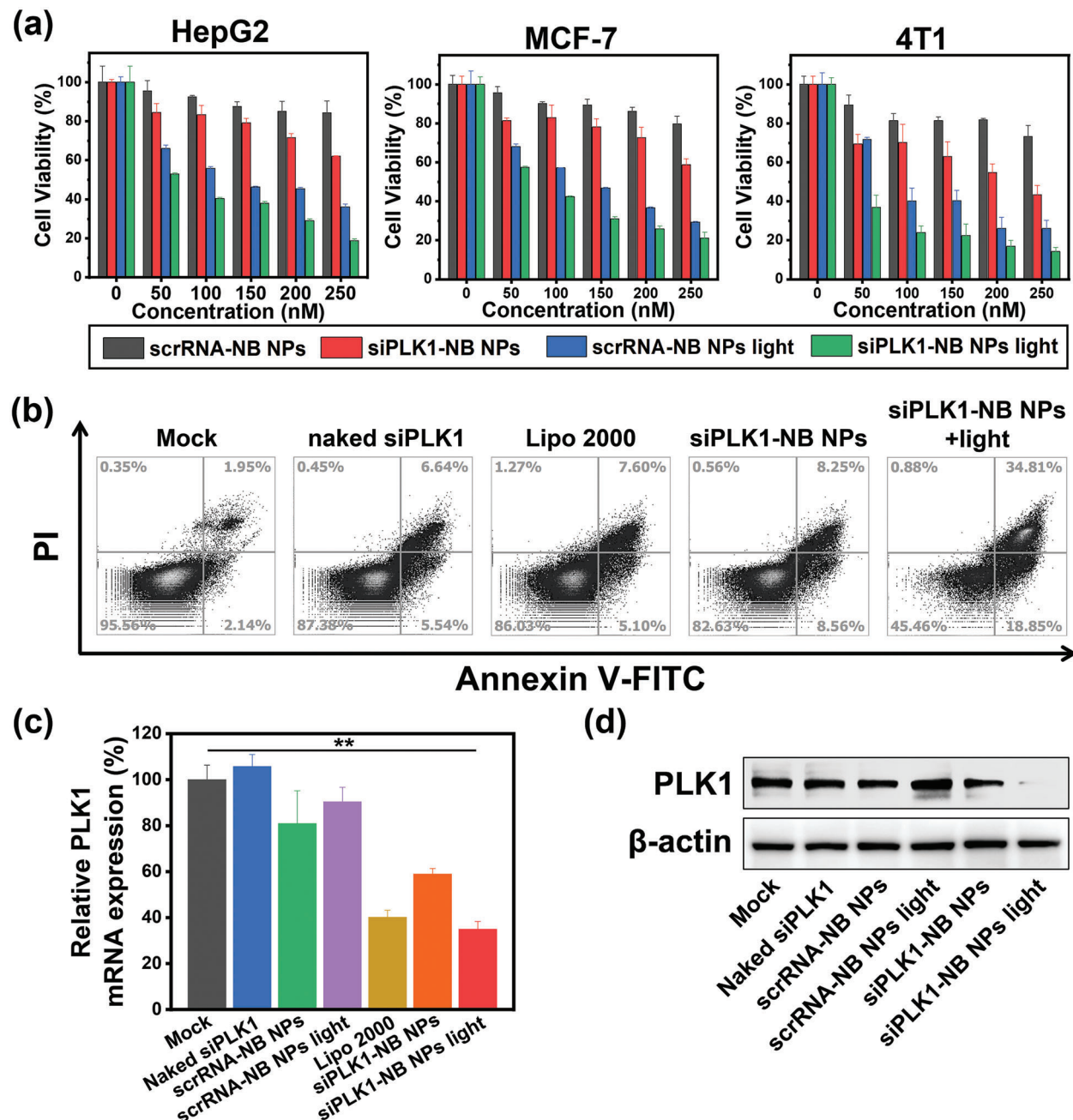


Figure 3. a) Survival rate of HepG2, MCF-7, and 4T1 cells after incubated with siPLK1-NB NPs or scrRNA-NB NPs at various concentrations in the dark or with light irradiation ($660\text{ nm}, 15\text{ mW cm}^{-2}, 10\text{ min}$). $n = 4$. b) Flow cytometry analysis of HepG2 cells after incubated with naked siPLK1, siPLK1 transfected by Lipofectamine 2000, and siPLK1-NB NPs without or with 660 nm irradiation ($15\text{ mW cm}^{-2}, 5\text{ min}$) at the equivalent siPLK1 concentration of 200 nM . c) PLK1 mRNA expression level in HepG2 cells, in which untreated HepG2 cells were used as controls. $n = 3$. d) PLK1 expression in HepG2 cells after treatment with naked siPLK1, scrRNA-NB NPs, scrRNA-NB NPs + light, siPLK1-NB NPs, siPLK1-NB NPs + light with a siRNA concentration of 100 nM . NIR light irradiation ($660\text{ nm}, 15\text{ mW cm}^{-2}, 5\text{ min}$) was conducted. Data were expressed as mean \pm SD, $^{**}p < 0.01$ determined by Student's *t* test.

and HepG2-tumor-bearing BALB/cA nude mice. As shown in Figure 4d,e, all of the fluorescence intensities were gradually increased and primarily accumulated in liver and tumor tissues, peaking at 2 h post-injection. As expected, in the HepG2-tumor-bearing nude mice, stronger fluorescence of siPLK1-NB NPs was observed in the tumor site than in the liver at 2 h post-injection

(Figure 4f). All these above results demonstrated that siPLK1-NB NPs had effective tumor accumulation ability due to its special internal charge adjustment and the EPR effect. Furthermore, in order to evaluate the delivery efficiency of siPLK1-NB NPs, the fluorescence imaging and relative intensities of HepG2-tumor-bearing nude mice were evaluated after intratumoral and intra-

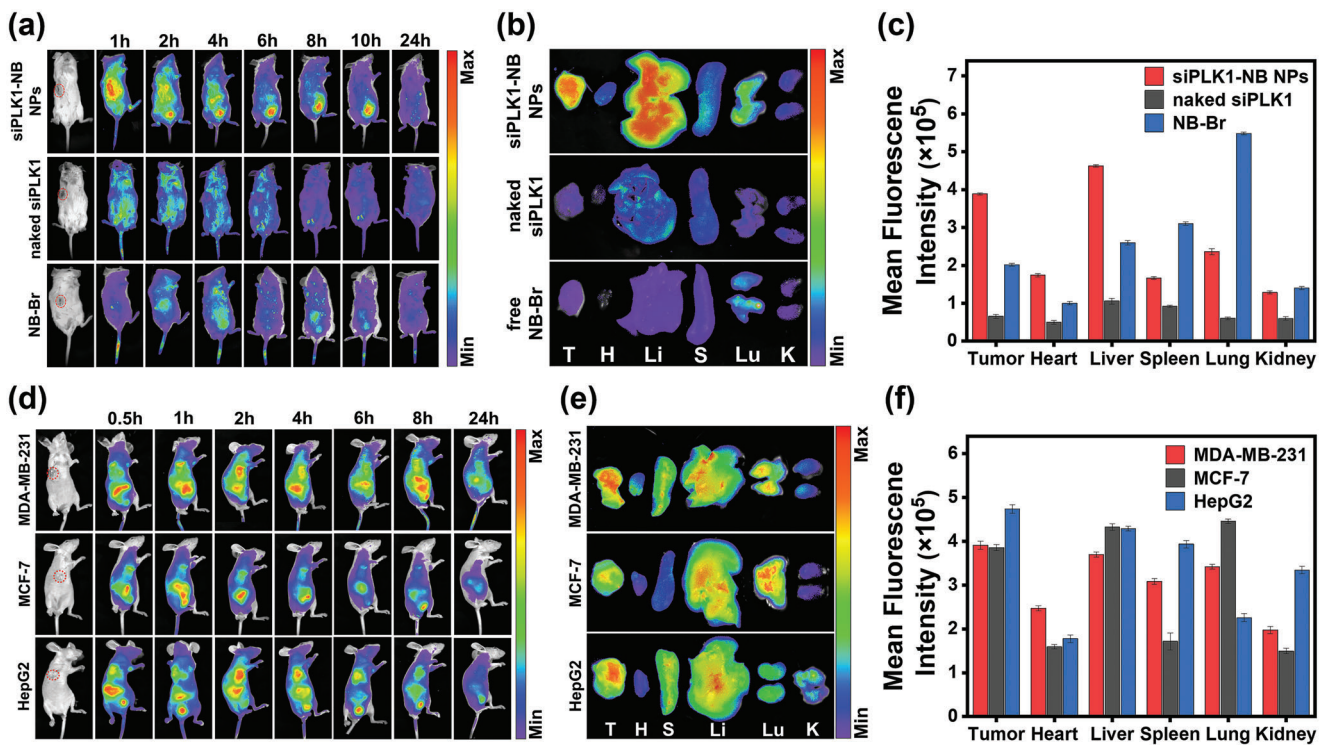


Figure 4. In vivo tumor targeting and biodistribution of siPLK1-NB NPs. a) In vivo imaging of siPLK1-NB NPs, FAM-labelled naked siPLK1 and free NB-Br in 4T1-tumor-bearing BALB/c mice. b) In vivo biodistribution of major organs after different treatments at 1 h post-injection—T: tumor; H: heart; Li: liver; S: spleen; Lu: lung; K: kidney. c) Quantitative accumulations of siPLK1-NB NPs, FAM-labeled naked siPLK1 and free NB-Br in major organs and tumors after 1 h post-injection. d) In vivo imaging of siPLK1-NB NPs in MDA-MB-231-tumor-bearing BALB/cA nude mice, MCF-7-tumor-bearing BALB/cA nude mice and HepG2-tumor-bearing BALB/cA nude mice. e) In vivo biodistribution of major organs after different treatments at 2 h post-injection—T: tumor; H: heart; Li: liver; S: spleen; Lu: lung; K: kidney. f) Quantitative accumulations of the above three formulations in major organs and tumors after 2 h post-injection. Error bars, mean \pm SD ($n = 3$).

venous injections of siPLK1-NB NPs at 2 h post-injection. Notably, the delivery efficiency of intravenous injection was $\approx 36\%$ compared to intratumoral injection (Figure S10, Supporting Information), demonstrating the outstanding in vivo delivery efficiency of siPLK1-NB NPs for gene therapy.

Based on the above-mentioned encouraging results, we further investigated the in vivo antitumor efficacy of siPLK1-NB NPs. When the tumor volume in the HepG2-tumor-bearing nude mice model reached $\approx 100 \text{ mm}^3$, the mice were randomly divided into six groups: PBS, PBS + light, scrRNA-NB NPs, scrRNA-NB NPs + light, siPLK1-NB NPs and siPLK1-NB NPs + light. HepG2-tumor-bearing nude mice were intravenously injected with PBS, scrRNA-NB NPs and siPLK1-NB NPs, respectively, on Day 0 and Day 3 (siRNA dose: 4 nmol). The tumor regions of nude mice in the light groups were irradiated with 660 nm light (50 mW cm^{-2} , 5 min) after 2 h post-injection. Mice in the dark group were injected with the same volume of PBS, scrRNA-NB NPs or siPLK1-NB NPs without light irradiation. The tumor volume and body weight were recorded every 2 days. After all treatments, all of the mice were euthanized, and tumors were collected for weighing and imaging (Figure 5a). As shown in Figure 5b, tumors in the PBS-treated group grew remarkably during the treatment regardless of light irradiation (tumor growth of approximately eightfold), suggesting the little influence of NIR light irradiation on tumor inhibition. The dark group of scrRNA-NB NPs-treated

mice also showed no tumor suppression behavior, confirming that scrRNA-NB NPs had negligible toxicity. For the scrRNA-NB NPs group under 660 nm light (50 mW cm^{-2} , 5 min), tumor growth inhibition was observed after 12 days of treatment, indicating that scrRNA-NB NPs were effective for PDT. Benefiting from the capability to inhibit tumor cell proliferation via knocking down PLK1 expression, the “siPLK1-NB NPs” group demonstrated a tumor inhibition rate of close to 30%. Remarkably, compared with other groups, siPLK1-NB NPs under 660 nm light irradiation showed the most efficient inhibitory ability on tumor volume and weight due to the synergistic effects of gene therapy and PDT (Figure 5b,d). The representative images also confirmed the excellent antitumor performance (Figure S11, Supporting Information). Moreover, the staining results of tumor sections showed that the cell nuclei were shrunken or broken, and almost no cells with complete morphology were observed in the siPLK1-NB NPs + light group, suggesting its effective tumor suppression (Figure 5f). No abnormal change was observed in the body weight of mice in each group during the course of treatment, hinting the biosafety of treatments for animals (Figure 5c). A western blot assay was further used to analyze the PLK1 protein expression levels of tumors after different treatments. Encouragingly, tumor in siPLK1-NB NPs + light group exhibited severely limited expression level of PLK1 protein, indicating the excellent in vivo gene silencing capability of siPLK1-NB NPs.

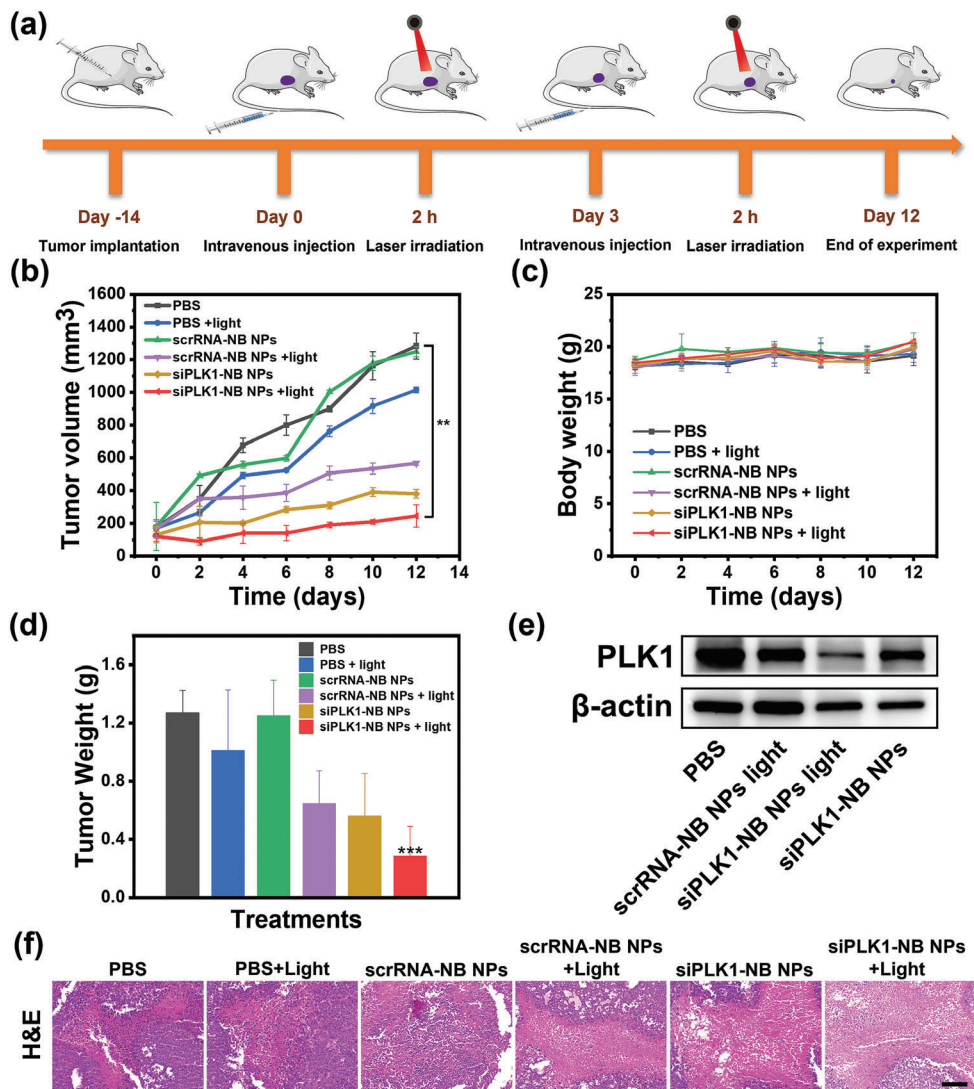


Figure 5. In vivo antitumor efficacy of siPLK1-NB NPs in HepG2-tumor-bearing BALB/cA-nude mice. a) Schematic illustration of the treatment schedule. b) The tumor growth curves during the treatment. c) Body weights for mice in six treatment groups. d) Tumor weights for mice in six treatment groups. e) Western blotting analyses of PLK1 protein levels in tumor tissues after different treatments. f) H&E staining of tumor sections from mice after different treatments. Scale bar = 100 μm . Data are shown as mean \pm SD ($n = 3$), ** $p < 0.01$, *** $p < 0.001$ determined by a Student's t-test.

To further evaluate the biosafety of siPLK1-NB NPs, major organs, including the heart, liver, spleen, lung, and kidney were collected and subjected to hematoxylin and eosin (H&E) staining after treatment. No distinguishable changes were observed in these organs in the treated groups, indicating the good biosafety and biocompatibility of siPLK1-NB NPs (Figure S12, Supporting Information). In addition, serum biochemistry assays were conducted after administering siPLK1-NB NPs to mice. As shown in Figure S13 (Supporting Information), levels of alanine aminotransferase, aspartate aminotransferase, blood urea nitrogen, and creatinine did not show any significant change, indicating that the treatment had no impact on liver and kidney functions. These results collectively confirmed the biocompatibility and biosafety of the siPLK1-NB NPs for synergistic antitumor treatment.

3. Conclusion

We have designed an electrostatic attraction-driven carrier-free siRNA delivery NPs by grafting cationic sulfur-substituted Nile Blue photosensitizer (NB-Br) onto deblock siRNA strands. Without the aid of any polymeric components, siPLK1-NB NPs could accumulate at the tumor site after systemic administration and efficiently enter tumor cells. Under light irradiation, the ROS generated by NB-Br could destroy the lysosome structure and promote siRNA escape from lysosomes. Moreover, the ROS could further induce tumor cell apoptosis. siPLK1-NB NPs could suppress the target PLK1 gene under light irradiation both in vitro and in vivo, achieving the RNAi and PDT synergistic cancer treatment. Our design of a carrier-free siRNA delivery system presents great potential to achieve light-induced self-delivery of

siRNA, which has been demonstrated in both cell and mouse models. We strongly believe that siRNA-NB NPs can be used as a nanoplatform for the self-delivery of siRNA drugs. Our next step is to develop a novel strategy for promoting siRNA to escape from lysosomes without the aid of cationic polymers or ROS.

Supporting Information

Supporting Information is available from the Wiley Online Library or from the author.

Acknowledgements

This work was financially supported by National Natural Science Foundation of China (21925802), the Fundamental Research Funds for the Central Universities (DUT22LAB601), Basic Research Fund for Free Exploration (2021Sszvup019) and NSFC-Liaoning United Fund (U1908202). All animal procedures were performed in accordance with the guidelines for Care and Use of Laboratory Animals of Dalian Medical University, and approved by the Dalian University of Technology Animal Care and Use Committee (DUT20230322).

Conflict of Interest

The authors declare no conflict of interest.

Data Availability Statement

The data that support the findings of this study are available from the corresponding author upon reasonable request.

Keywords

gene therapy, lysosome escape, photodynamic therapy, self-delivery, siRNA

Received: February 13, 2023

Revised: April 16, 2023

Published online: June 9, 2023

- [1] B. L. Davidson, P. B. McCray, *Nat. Rev. Genet.* **2011**, *12*, 329.
- [2] Y. Jr, M. Ariful, *Sci. Transl. Med.* **2020**, *13*.
- [3] A. Gallas, C. Alexander, M. C. Davies, S. Puri, S. Allen, *Chem. Soc. Rev.* **2013**, *42*, 7983.
- [4] M. Zhang, Y. Weng, Z. Cao, S. Guo, B. Hu, M. Lu, W. Guo, T. Yang, C. Li, X. Yang, Y. Huang, *ACS Appl. Mater. Interfaces* **2020**, *12*, 32289.
- [5] J. D. Torres-Vanegas, J. C. Cruz, L. H. Reyes, *Pharmaceutics* **2021**, *13*, 428.
- [6] H. Xue, F. Ding, J. Zhang, Y. Guo, X. Gao, J. Feng, X. Zhu, C. Zhang, *Chem. Commun.* **2019**, *55*, 4222.
- [7] J. P. Bost, H. Barriga, M. N. Holme, A. Gallud, M. Maugeri, D. Gupta, T. Lehto, H. Valadi, E. K. Esbjörner, M. M. Stevens, S. El-Andaloussi, *ACS Nano* **2021**, *15*, 13993.
- [8] M. Everts, V. Saini, J. L. Leddon, R. J. Kok, M. Stoff-Khalili, M. A. Preuss, C. L. Millican, G. Perkins, J. M. Brown, H. Bagaria, D. E. Nikles, D. T. Johnson, V. P. Zharov, D. T. Curiel, *Nano Lett.* **2006**, *6*, 587.
- [9] C. Wang, X. Wang, L. Du, Y. Dong, B. Hu, J. Zhou, Y. Shi, S. Bai, Y. Huang, H. Cao, Z. Liang, A. Dong, *ACS Appl. Mater. Interfaces* **2021**, *13*, 2218.
- [10] O. B. Garbuzenko, M. Saad, V. P. Pozharov, K. R. Reuhl, G. Mainelis, T. Minko, *Proc. Natl. Acad. Sci. USA* **2010**, *107*, 10737.
- [11] Y. Zhao, R. Li, J. Sun, Z. Zou, F. Wang, X. Liu, *ACS Nano* **2022**, *16*, 5404.
- [12] A. Akinc, M. A. Maier, M. Manoharan, K. Fitzgerald, M. Jayaraman, S. Barros, S. Ansell, X. Du, M. J. Hope, T. D. Madden, B. L. Mui, S. C. Semple, Y. K. Tam, M. Ciufolini, D. Witzigmann, J. A. Kulkarni, R. van der Meel, P. R. Cullis, *Nat. Nanotechnol.* **2019**, *14*, 1084.
- [13] J. I. Cutler, E. Auyeung, C. A. Mirkin, *J. Am. Chem. Soc.* **2012**, *134*, 1376.
- [14] N. L. Rosi, D. A. Giljohann, C. S. Thaxton, A. K. R. Lytton-Jean, M. S. Han, C. A. Mirkin, *Science* **2006**, *312*, 1027.
- [15] C. H. J. Choi, L. Hao, S. P. Narayan, E. Auyeung, C. A. Mirkin, *Proc. Natl. Acad. Sci. USA* **2013**, *110*, 7625.
- [16] J. Gilleron, W. Querbes, A. Zeigerer, A. Borodovsky, G. Marsico, U. Schubert, K. Manygoats, S. Seifert, C. Andree, M. Stöter, H. Epstein-Barash, L. Zhang, V. Koteliantsky, K. Fitzgerald, E. Fava, M. Bickle, Y. Kalaidzidis, A. Akinc, M. Maier, M. Zerial, *Nat. Biotechnol.* **2013**, *31*, 638.
- [17] C. Li, J. Zhou, Y. Wu, Y. Dong, L. Du, T. Yang, Y. Wang, S. Guo, M. Zhang, A. Hussain, H. Xiao, Y. Weng, Y. Huang, X. Wang, Z. Liang, H. Cao, Y. Zhao, X.-J. Liang, A. Dong, Y. Huang, *Nano Lett.* **2021**, *21*, 3680.
- [18] L. Shi, W. Wu, Y. Duan, L. Xu, S. Li, X. Gao, B. Liu, *ACS Nano* **2021**, *15*, 1841.
- [19] B. Ballarín-González, K. A. Howard, *Adv. Drug Delivery Rev.* **2012**, *64*, 1717.
- [20] F. Ding, Q. Mou, Y. Ma, G. Pan, Y. Guo, G. Tong, C. H. J. Choi, X. Zhu, C. Zhang, *Angew. Chem., Int. Ed.* **2018**, *57*, 3064.
- [21] L. Zhu, Y. Guo, Q. Qian, D. Yan, Y. Li, X. Zhu, C. Zhang, *Angew. Chem., Int. Ed.* **2020**, *59*, 17944.
- [22] Y. Guo, Q. Zhang, Q. Zhu, J. Gao, X. Zhu, H. Yu, Y. Li, C. Zhang, *Sci. Adv.* **2022**, *8*, eabn2941.
- [23] C. Ji, H. Li, L. Zhang, P. Wang, Y. Lv, Z. Sun, J. Tan, Q. Yuan, W. Tan, *Angew. Chem., Int. Ed.* **2022**, *61*, e202200237.
- [24] M. Li, Y. Shao, J. H. Kim, Z. Pu, X. Zhao, H. Huang, T. Xiong, Y. Kang, G. Li, K. Shao, J. Fan, J. W. Foley, J. S. Kim, X. Peng, *J. Am. Chem. Soc.* **2020**, *142*, 5380.
- [25] L. Shi, W. Wu, Y. Duan, L. Xu, Y. Xu, L. Hou, X. Meng, X. Zhu, B. Liu, *Angew. Chem., Int. Ed.* **2020**, *59*, 19168.
- [26] A. Khvorova, J. K. Watts, *Nat. Biotechnol.* **2017**, *35*, 238.
- [27] Y. Guo, J. Zhang, F. Ding, G. Pan, J. Li, J. Feng, X. Zhu, C. Zhang, *Adv. Mater.* **2019**, *31*, 1807533.
- [28] X. Zhao, S. Long, M. Li, J. Cao, Y. Li, L. Guo, W. Sun, J. Du, J. Fan, X. Peng, *J. Am. Chem. Soc.* **2020**, *142*, 1510.
- [29] M. Li, T. Xiong, J. Du, R. Tian, M. Xiao, L. Guo, S. Long, J. Fan, W. Sun, K. Shao, X. Song, J. W. Foley, X. Peng, *J. Am. Chem. Soc.* **2019**, *141*, 2695.
- [30] S. Liang, X.-Z. Yang, X.-J. Du, H.-X. Wang, H.-J. Li, W.-W. Liu, Y.-D. Yao, Y.-H. Zhu, Y.-C. Ma, J. Wang, E.-W. Song, *Adv. Funct. Mater.* **2015**, *25*, 4778.
- [31] J. Han, Y. Cui, F. Li, Z. Gu, D. Yang, *Nano Today* **2021**, *39*, 101160.
- [32] J. Zhang, Y. Guo, F. Ding, G. Pan, X. Zhu, C. Zhang, *Angew. Chem., Int. Ed.* **2019**, *58*, 13794.
- [33] Y. Zou, X. Sun, Y. Wang, C. Yan, Y. Liu, J. Li, D. Zhang, M. Zheng, R. S. Chung, B. Shii, *Adv. Mater.* **2020**, *32*, 2000416.
- [34] Q. Cheng, T. Wei, L. Farbiak, L. T. Johnson, S. A. Dilliard, D. J. Siegwart, *Nat. Nanotechnol.* **2020**, *15*, 313.
- [35] M. Li, J. Xia, R. Tian, J. Wang, J. Fan, J. Du, S. Long, X. Song, J. W. Foley, X. Peng, *J. Am. Chem. Soc.* **2018**, *140*, 14851.

- [36] Z. Shu, I. Tanaka, A. Ota, D. Fushihara, N. Abe, S. Kawaguchi, K. Nakamoto, F. Tomoike, S. Tada, Y. Ito, Y. Kimura, H. Abe, *Angew. Chem., Int. Ed.* **2019**, *58*, 6611.
- [37] V. Martinez, M. Henary, *Chemistry* **2016**, *22*, 13764.
- [38] L. Chen, G. Li, X. Wang, J. Li, Y. Zhang, *ACS Nano* **2021**, *15*, 11929.
- [39] Y. Weng, H. Xiao, J. Zhang, X.-J. Liang, Y. Huang, *Biotechnol. Adv.* **2019**, *37*, 801.